Appendix D

KINETICS AND PRODUCTS OF THE REACTION OF THE FIRST-GENERATION ISOPRENE HYDROXY HYDROPEROXIDE (ISOPOOH) WITH OH

St. Clair, J. M., J. C. Rivera-Rios, J. D. Crounse, H. C. Knap, K. H. Bates, A. P. Teng, S. Jorgensen, H. G. Kjaergaard, F. N. Keutsch, and P. O. Wennberg (2015). "Kinetics and products of the reaction of the first-generation isoprene hydroxy hydroperoxide (ISOPOOH) with OH". In: *J. Phys. Chem. A* 120.9, pp. 1441–1451. DOI: 10.1021/acs.jpca.5b06532.

Abstract

The atmospheric oxidation of isoprene by the OH radical leads to the formation of several isomers of an unsaturated hydroxy hydroperoxide, ISOPOOH. Oxidation of ISOPOOH by OH produces epoxydiols, IEPOX, which have been shown to contribute mass to secondary organic aerosol (SOA). We present kinetic rate constant measurements for OH + ISOPOOH using synthetic standards of the two major isomers: (1,2)- and (4,3)-ISOPOOH. At 297 K, the total OH rate constant is $7.5 \pm 1.2 \times 10^{-11}$ cm^3 molecule^{-1} s^{-1} for (1,2)-ISOPOOH and $1.18 \pm 0.19 \times 10^{-10}$ cm^3 molecule^{-1} s^{-1} for (4,3)-ISOPOOH. Abstraction of the hydroperoxy hydrogen accounts for approximately 12% and 4% of the reactivity for (1,2)-ISOPOOH and (4,3)-ISOPOOH, respectively. The sum of all H-abstractions account for approximately 15% and 7% of the reactivity for (1,2)-ISOPOOH and (4,3)-ISOPOOH, respectively. The major product observed from both ISOPOOH isomers was IEPOX (*cis*-β and *trans*-β isomers), with a ~2:1 preference for *trans*-β IEPOX and similar total yields from each ISOPOOH isomer (~70-80%). An IEPOX global production rate of more than 100 Tg C each year is estimated from this chemistry using a global 3D chemical transport model, similar to earlier estimates. Finally, following addition of OH to ISOPOOH, approximately 13% of the reactivity proceeds *via* addition of O_2 at 297 K and 745 Torr. In the presence of NO, these peroxy radicals lead to formation of small carbonyl compounds. Under HO_2 dominated chemistry, no products are observed from these channels. We suggest that the major products, highly oxygenated organic peroxides, are lost to the chamber walls. In the atmosphere, formation of these compounds may contribute to organic aerosol mass.

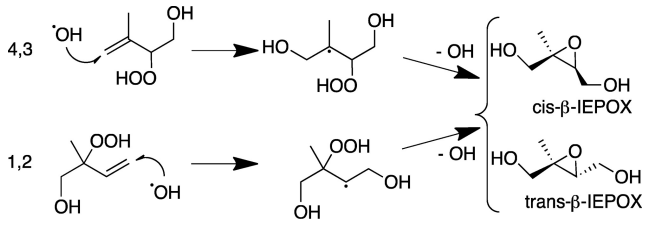

Figure D.1: Mechanism for the formation of *cis*- and *trans*-β-IEPOX from OH addition to (4,3)- and (1,2)-ISOPOOH.

D.1 Introduction

Global emissions of isoprene (2-methyl-1,3-butadiene, C_5H_8, ISOP) are estimated to be ~540 Tg (~470 Tg C) each year (reference year 2000) and are the single largest source of atmospheric nonmethane hydrocarbons (Guenther *et al.*, 2006; Guenther *et al.*, 2012). Emissions from tropical broadleaf trees and other deciduous plants dominate the source (Guenther *et al.*, 2006; Guenther *et al.*, 2012). The oxidation of isoprene and its oxidation products by OH results in the formation of ozone and secondary organic aerosol (SOA), with impacts on human health and climate. The chemical fate of isoprene and its oxidative products also affects the abundance of OH in regions influenced by biological emissions (Archibald *et al.*, 2010; Lelieveld *et al.*, 2008).

Organic peroxy radicals, hereafter RO_2, formed from OH and subsequent O_2 addition to isoprene generally follow one of three reaction pathways: (1) reaction with HO_2 to form hydroperoxides (Crutzen *et al.*, 2000; Paulot *et al.*, 2009b); (2) reaction with NO to form hydroxynitrates or formaldehyde and methyl vinyl ketone (MVK)/methacrolein (MACR) and HO_2 (Paulot *et al.*, 2009a); (3) RO_2 H-shift isomerization of the RO_2 radicals followed by reaction with O_2 to form hydroperoxyenals (HPALDs) and other oxidized products (Crounse *et al.*, 2011; Peeters *et al.*, 2009; Wolfe *et al.*, 2012). The fate of the RO_2 is dependent on the concentrations of HO_2, NO, RO_2, and the temperature. Under HO_2-dominated conditions, the main products are unsaturated hydroperoxides (several isomers, collectively referred to as ISOPOOH):

$ISOP + OH + O_2 \rightarrow ISOPOO\cdot$

$ISOPOO\cdot + HO_2 \rightarrow ISOPOOH$

As illustrated in Figure D.1, a subsequent reaction of ISOPOOH with OH can produce epoxydiols (several isomers, collectively referred to as IEPOX) and recycle OH (Paulot *et al.*, 2009b).

IEPOX was proposed as an SOA precursor (Paulot *et al.*, 2009b; Surratt *et al.*, 2010), and has subsequently been shown to contribute to SOA mass in field (Budisulistiorini *et al.*, 2013; Froyd *et al.*, 2011; Worton *et al.*, 2013) and laboratory (Gaston *et al.*, 2014; Lin *et al.*, 2012; Liu *et al.*, 2015; Nguyen *et al.*, 2014a) measurements. Recent laboratory studies of gas phase oxidation of IEPOX by OH (Bates *et al.*, 2014; Jacobs *et al.*, 2013) and of IEPOX aerosol uptake properties (Gaston *et al.*, 2014; Lin *et al.*, 2012; Liu *et al.*, 2015; Nguyen *et al.*, 2014a) were made possible by the development of synthetic routes to IEPOX (Zhang *et al.*, 2012).

Previously, estimates of the OH + ISOPOOH rate coefficients and products were inferred from OH + isoprene experiments, with limited ability to elucidate the relative role of the different isomers of ISOPOOH (Paulot *et al.*, 2009b). Here, using synthetic ISOPOOH standards (Rivera-Rios *et al.*, 2014), we report kinetic rate constant measurements for the OH + ISOPOOH reaction, relative to OH + propene, for the two main isomers, (1-OH,2-OOH)-ISOPOOH (hereafter (1,2)-ISOPOOH) and (4-OH,3-OOH)-ISOPOOH (hereafter (4,3)-ISOPOOH) (Figure D.1). The products of this chemistry were also determined. The impact of updating the low NO isoprene mechanism on the global production of IEPOX was explored using the GEOS-Chem chemical transport model.

D.2 Experimental Methods

The environmental chamber and techniques used for these experiments have been described previously (Bates *et al.*, 2014; Crounse *et al.*, 2013; Lee *et al.*, 2014), with study-specific details provided below. A gas chromatograph with a flame ionization detector (GC-FID, Hewlett-Packard 5890 series II Plus) was used to measure propene for the relative rate kinetics experiments. Measurements of ISOPOOH and its oxidation products were made using two CF_3O^- chemical ionization mass spectrometers (CIMS), which have been described previously (Crounse *et al.*, 2006; Paulot *et al.*, 2009a; St. Clair *et al.*, 2010). CF_3O^- selectively ionizes analytes to typically form either an ion cluster (*m/z* = analyte mass +85) or a fluoride *trans*fer ion (*m/z* = analyte mass +19). The time-of-flight CIMS (ToF-CIMS) provided 1 Hz unit mass data for *m/z* = 19 to *m/z* = 396. The triple quadrupole CIMS (TQ-CIMS) was operated exclusively in tandem MS mode to differentiate the cluster ion *m/z* = 203 signal from the two isobaric compounds, ISOPOOH and IEPOX (Paulot *et al.*, 2009b). The signal observed at *m/z* = 203 → *m/z* = 63 arises primarily from ISOPOOH while the signal at *m/z* = 203 → *m/z* = 183 is primarily from IEPOX.

expt #	$[ISOPOOH]_0$ (ppbv)	$[propene]_0$ (ppbv)	$[H_2O_2]_0$ (ppmv)	$[NO]_0$ (ppbv)	reaction time (h)
K1	210	61	2.2	515	1.7
K2	108	76	1.9	518	1.7
K3	15	68	1.8	514	2.4
K4	18	66	2.2	513	3.0
K5	23	77	2.1	539	2.0
K6	51	116	2.1	513	2.1
K7	45	161	2.0	515	2.5
K8	41	183	2.2	507	1.7
K9	31	166	2.2	510	1.8

Table D.1: Experimental conditions for OH + ISOPOOH kinetics experiments.

All experiments were conducted in a 0.85 m^3 chamber made of fluorinated ethylene propylene (Teflon-FEP, DuPont) with one port for the introduction of reagents and sampling. During an experiment, approximately 1 std L min^{-1} of sample flow was drawn from the bag *via* a 6.35 mm O.D. PFA tube, with the CIMS instruments subsampling the main tube flow *via* glass orifices. The chamber was at 297 ± 2 K and 745 Torr (99.3 kPa) for all experiments.

The chamber was prepared for each experiment with multiple flushes of dry air from a purge gas generator (Perkin, model 75-52). H_2O_2, the OH source, was added first to the bag by flowing 20 std L min^{-1} of dry air over ~5 μL of 50% H_2O_2 contained in a shallow glass vial for 12 min, resulting in ~2 ppmv in the final mixture. The addition of ISOPOOH followed, with 1-2 min of dry air at 20 std L min^{-1} passed over ISOPOOH in a shallow glass vial. For the HO_2-dominated experiments, the remainder of the bag volume was filled with dry air. For NO-dominated kinetics experiments, propene was added next, with NO added once the bag was nearly full to minimize conversion to NO_2. Propene (Sigma-Aldrich, ≥99%) was prepared for addition by obtaining a ~300 ppmv propene sample in a 500 cm^3 glass flask at room pressure using pure propene and serial dilution. The mixing ratio of the ~300 ppmv propene sample was verified using FT-IR and tabulated propene cross section (Johnson *et al.*, 2002; Sharpe *et al.*, 2004). NO was prepared by adding ~330 Torr of 2000 ppmv NO (Matheson Gas Products) to a 500 cm^3 glass flask. Tables D.1 and D.2 contain the details for each high NO and low NO experiment, respectively.

Kinetics experiments were conducted using four of the eight available UV lights ($J_{NO_2} \approx 1 \times 10^{-3}$ s^{-1}). At least 2/3 of the ISOPOOH was oxidized in each experiment,

expt #	$[ISOPOOH]_0$ (ppbv)	$[H_2O_2]_0$ (ppmv)	% ISOPOOH reacted
Y1	119	2.0	9
Y2	25	1.8	12
Y3	21	1.9	13
Y4	22	2.1	15
Y5	33	2.1	9
Y6	25	2.0	12
Y7	21	1.9	15
Y8	45	2.2	12
Y9	36	2.2	9
Y10	34	2.2	17
Y11	37	2.2	33

Table D.2: Experimental conditions for OH + ISOPOOH product yield experiments.

requiring 1.5-3 h of photo-oxidation. Low NO product yield experiments were run with all available lights, oxidizing only ~10% of the starting ISOPOOH to minimize the secondary loss of products to reaction with OH and to the walls. Before and after the oxidation, GC-ToF-CIMS chromatograms were collected to aid in product identification (Bates *et al.*, 2014). Product yields were determined by dividing the change in the product mixing ratio ($X_{postoxidation}$ - $X_{preoxidation}$) by the change in the ISOPOOH mixing ratio. CF_3O^- CIMS sensitivities used to determine mixing ratios are included in the Supporting Information. Wall loss of ISOPOOH in the presence of H_2O_2 was determined before and after the oxidation during the kinetics experiments and was found to be negligible ($-1 \pm 1\%\ h^{-1}$). Previous work investigated the wall loss of IEPOX and found it to be small ($<-1\%\ h^{-1}$) in the absence of acid (Bates *et al.*, 2014).

The experiments used several different synthetic ISOPOOH batches with differing purities. The ISOPOOH samples used for experiments K8-K9 and Y8-Y11 had fewer impurities than those available for experiments K1-K7 and Y1-Y7. The main impurity was 2-methyl-1-butene-3,4-diol, observed in the CIMS instruments as a CF_3O^- cluster ion with *m/z* = 187, for the (4,3)-ISOPOOH and 3-methyl-1-butene-3,4-diol for the (1,2)-ISOPOOH. In the (4,3)-ISOPOOH samples used for experiments K1-K7 and Y1-Y7, the diol impurity signal was about 10% of the ISOPOOH signal; the impurity in the samples used in the last few experiments was only ~2%. For the (1,2)-ISOPOOH, the impurity signal was always small (1% in initial experiments, 0.5% in later). Other impurities included H_2O_2 and

two compounds that produce signal at *m/z* = 201 and *m/z* = 185, with the latter two assumed to be the same compounds as are produced from the OH oxidation of ISOPOOH (see products of ISOPOOH sections below). The ISOPOOH product yields were corrected for the methylbutenediol oxidation products, as discussed in the Supporting Information.

D.3 Results and Discussion

D.3.1 Kinetics

The kinetic rate coefficient of the ISOPOOH + OH reaction was determined relative to that of OH + propene for both (1,2)-ISOPOOH and (4,3)-ISOPOOH. The propene rate coefficient (2.59×10^{-11} cm^3 molecule^{-1} s^{-1} at 298 K) was obtained using the pressure dependence from the IUPAC recommendation and normalizing the rate constant to the Atkinson and Arey recommended rate constant (Atkinson and Arey, 2003b; Atkinson *et al.*, 2006). For each experiment, a linear regression (York *et al.*, 2004) was performed on $\log_e([\text{propene}]/[\text{propene}]_0)$ vs $\log_e([\text{ISOPOOH}]/[\text{ISOPOOH}]_0)$ data set (Figure D.2), with the ISOPOOH + OH reaction rate coefficient equal to the fitted slope divided by the propene rate constant. Table D.3 contains the rate constants determined for each experiment and the recommended rate constants for the two ISOPOOH isomers. The recommended rate constant was calculated by taking a mean from all the experiments weighted by their respective uncertainties. Uncertainties for all the ISOPOOH+OH rate constants include ±15% from the propene rate constant (Atkinson and Arey, 2003b). The rate constant uncertainty is dominated by the uncertainty in the propene rate constant, with the precision of the GC-FID measurement of propene dominating the fit uncertainty.

Estimates of the hydrogen abstraction rate constants were also obtained, using both the high NO kinetics experiments and the low NO product yield experiments (Tables D.4 and D.5). Both ISOPOOH isomers have labile hydrogens on the hydroperoxy group and α to the hydroxy group. (4,3)-ISOPOOH has, in addition, a hydrogen α to the hydroperoxy group. Removal of the hydroperoxy hydrogen produces the RO_2 that can reform the same ISOPOOH isomer upon reaction with HO_2. Standard chemistry suggests that abstraction of the hydrogen α to the hydroxy group will lead to a C_5-hydroperoxyenal (HPALD, *m/z* = 201) under low NO conditions (Figure D.3). The abstraction of the hydrogen α to the (4,3)-ISOPOOH hydroperoxy group is expected to form a β-C_5-hydroxy carbonyl (HC_5, *m/z* = 185) in a OH-neutral reaction (Figure D.4) (Vereecken *et al.*, 2004).

compound	experiment	rate $\times 10^{11}$ (cm^3 $molecule^{-1}$ s^{-1})
(1,2)-ISOPOOH	K3	7.49 ± 1.61
	K4	7.44 ± 1.31
	K5	7.84 ± 1.85
	K7	7.50 ± 1.36
		weighted mean: 7.5 ± 1.2
(4,3)-ISOPOOH	K1	12.6 ± 3.1
	K2	10.8 ± 2.7
	K6	11.7 ± 2.2
	K8	11.9 ± 2.6
	K9	12.0 ± 2.6
		weighted mean: 11.8 ± 1.9

Table D.3: OH + ISOPOOH kinetic rate coefficients.

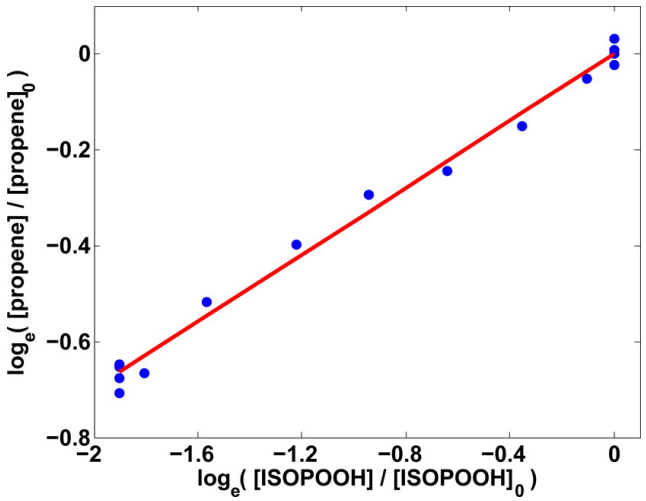

Figure D.2: Fit to the propene vs (1,2)-ISOPOOH decay to determine the ISOPOOH + OH rate relative to propene + OH for experiment K4. The slope in this experiment is 0.349 ± 0.032, with an ISOPOOH + OH rate of 7.44 ± 1.31 × 10^{-11} cm^3 $molecule^{-1}$ s^{-1}.

product	Y1	Y2	Y3	Y4	Y11	mean
hydroxyacetone	3.7	6.3	5.6	4.6	2.0	4.4
m/z = 189	3.3	3.4	3.6	3.5	2.1	3.2
m/z = 201	2.1	2.5	2.5	2.6	1.9	2.3
glycolic acid	1.3	1.6	1.7	2.0	0.6	1.4
m/z = 185	0.9	1.4	1.1	0.9	1.0	1.1
sum of non-IEPOX products	11.3	15.2	14.5	13.6	7.6	12.4

Table D.4: Reaction products from OH + (4,3)-ISOPOOH for HO_2-dominated conditions. Molar yields reported in percent.

product	Y5	Y6	Y7	Y8	Y9	Y10	mean
hydroxyacetone	1.3	1.0	1.5	1.4	1.2	1.5	1.3
m/z = 189	2.8	2.7	3.5	3.7	3.6	3.4	3.4
m/z = 201	1.5	1.7	2.1	2.1	2.2	1.9	2.0
m/z = 93	1.5	2.4	1.3	1.1	1.3	1.0	1.4
m/z = 161	1.1	0.8	1.3	1.1	1.3	0.9	1.1
m/z = 185	2.1	1.6	2.1	2.1	2.1	1.9	2.0
glycolaldehyde	0.7	0.8	1.0	1.2	0.7	0.9	0.9
sum of non-IEPOX products	11.4	11.4	13.2	12.7	12.4	11.5	12.1

Table D.5: Reaction products from OH + (1,2)-ISOPOOH for HO_2-dominated conditions. Yields reported in percent.

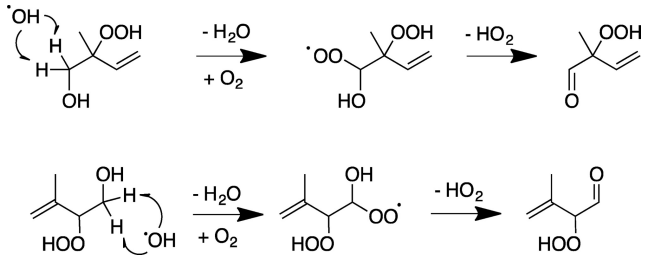

Figure D.3: Mechanism for the formation of HPALD (*m/z* = 201) from (1,2)-ISOPOOH (top) and (4,3)-ISOPOOH (bottom) by H-abstraction.

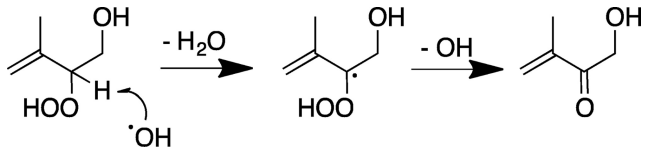

Figure D.4: Mechanism for the formation of a β-HC_5 (*m/z* = 185) from (4,3)-ISOPOOH by H-abstraction.

The yield of *m/z* = 185, presumed to be a β-hydroxy-carbonyl, HC_5, from (4,3)-ISOPOOH was low: ~1%. We also observed a compound at *m/z* = 185 from (1,2)-ISOPOOH with a yield of ~2%. However, because the (1,2)-ISOPOOH lacks a hydrogen α to the hydroperoxy group, it cannot form HC_5 *via* this route. One possibility is an epoxide, shown in Figure D.5. Alternatively, it is possible that HC_5 is formed from an impurity (such as (2,1)-ISOPOOH). Impurities at *m/z* = 185 and *m/z* = 201 were large enough that loss of the initial compound by reaction with OH affected the determination of yields, and consequently H-abstraction rate constants, from OH + ISOPOOH. An approximate correction for the loss by OH was applied using the approach of Atkinson *et al.* (1982). OH rate constants for both compounds

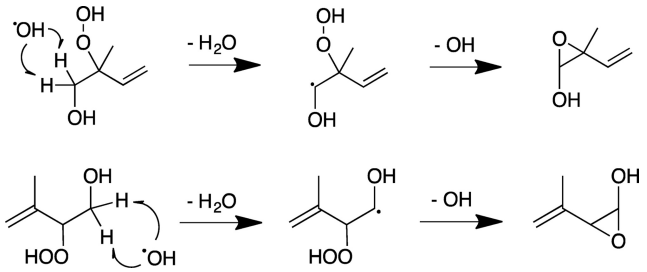

Figure D.5: Mechanism for the formation of an unsaturated hydroxy epoxide (*m/z* = 185) from (1,2)-ISOPOOH (top) and (4,3)-ISOPOOH (bottom) by H-abstraction. This channel is in competition with the chemistry illustrated in Figure D.3.

were assumed to be the same as the ISOPOOH standard.

The abstraction rate coefficient of the hydroperoxy hydrogen was determined using the observed formation of isoprene hydroxy nitrate (ISOPN, *m/z* = 232), which is formed from the product RO_2 under high NO conditions (Figure D.6). ISOPN CIMS sensitivities have been determined previously (Lee *et al.*, 2014; Teng *et al.*, 2015), and a 0.14 yield was used based on a currently unpublished best estimate. The ISOPN data were corrected for loss by OH (Atkinson *et al.*, 1982) and the slope of (ISOPN/Y_{ISOPN}) vs ISOPOOH was multiplied by the total ISOPOOH + OH rate constant to give the hydroperoxy hydrogen abstraction rate constant (Table D.6). We find that this channel is 12% of the overall OH reactivity for the (1,2)-ISOPOOH and 4% for the (4,3)-ISOPOOH, assuming equal Y_{ISOPN} for each isomer. From the sum of the H-abstraction rate constants determined *via* the formation rate of the *m/z* = 185 and *m/z* = 201 products, plus the lower uncertainty hydroperoxy hydrogen abstraction rate constant, we infer that the overall H-abstraction rate constants are 1.2×10^{-11} cm^3 molecule^{-1} s^{-1} for (1,2)-ISOPOOH and 8×10^{-12} cm^3 molecule^{-1} s^{-1} for (4,3)-ISOPOOH.

From the isomer specific rate coefficients determined here, and assuming an ambient ISOPOOH distribution as 67% (1,2)-ISOPOOH, 29% (4,3)-ISOPOOH, and 4% δ-ISOPOOH (Bates *et al.*, 2014), the isomer-averaged OH addition rate constant is 7.8×10^{-11} cm^3 molecule^{-1} s^{-1} and the isomer-averaged H-abstraction rate constant is 1.1×10^{-11} cm^3 molecule^{-1} s^{-1}. This can be compared with the results of Paulot *et al.* (2009b), who estimated the OH addition rate constant to ISOPOOH as 7.0×10^{-11} cm^3 molecule^{-1} s^{-1} and the H-abstraction rate constant as 7×10^{-12} cm^3 molecule^{-1} s^{-1}, both at 298 K.

compound	experiment	rate × 10^{12} (cm^3 $molecule^{-1}$ s^{-1})
(1,2)-ISOPOOH	K3	8.59 ± 1.59
	K4	8.91 ± 1.46
	K5	8.68 ± 1.43
	K7	9.38 ± 1.54
		weighted mean: 9.0 ± 1.4
(4,3)-ISOPOOH	K1	4.30 ± 0.70
	K2	4.01 ± 0.65
	K6	5.34 ± 0.89
	K8	4.23 ± 0.69
	K9	3.89 ± 0.63
		weighted mean: 4.2 ± 0.7

Table D.6: OH + ISOPOOH hydroperoxy H-abstraction rate coefficients.

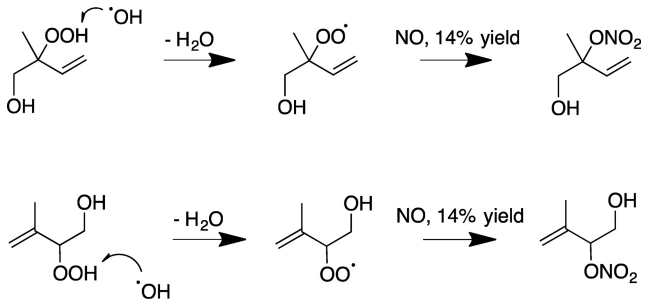

Figure D.6: Mechanism for the formation of isoprene β-hydroxynitrate (m/z = 232) from (1,2)-ISOPOOH (top) and (4,3)-ISOPOOH (bottom) following abstraction of the hydroperoxy hydrogen.

D.3.2 Products of OH Addition to (4,3)-ISOPOOH

OH addition to the internal carbon of the double bond, as well as external OH addition followed by O_2 addition to the alkyl radical, will result in products other than IEPOX. The formation of aldehydes and ketones in the high NO experiments provides a constraint on the amount of ISOPOOH that does not yield IEPOX after OH addition. A summary of these mechanisms is shown in Figures D.7 and D.8.

Following OH addition at C1 and O_2 addition at C2 of (4,3)-ISOPOOH, glycolaldehyde is expected to be produced as the primary product of the reaction of the peroxy radical with NO. Its yield will be matched by hydroxyacetone (Figure D.7). Additionally, a minor yield of five-carbon dihydroxy hydroperoxy nitrate is expected. Experiments K6, K8, and K9 were used for study of (4,3)-ISOPOOH. The glycolaldehyde and hydroxyacetone yields were corrected for production from

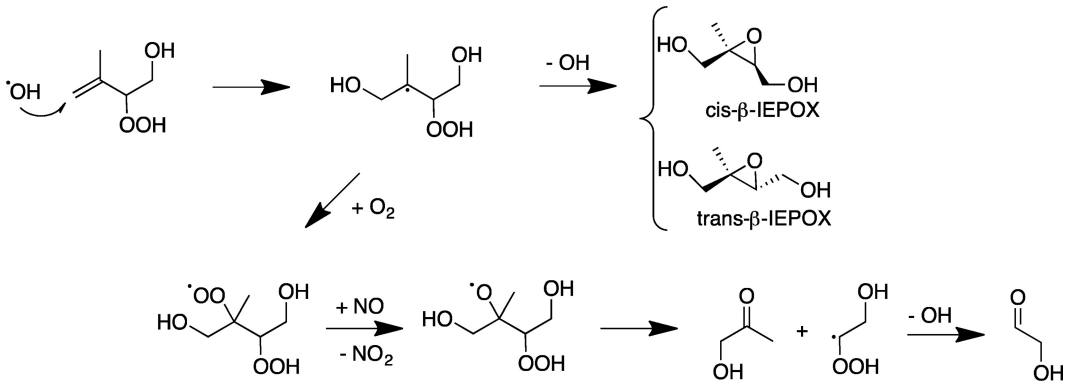

Figure D.7: External OH addition mechanism for (4,3)-ISOPOOH under high [NO]. Owing to the fast H-shift between RO_2 groups, the peroxy radical that reacts with NO may be on C3 rather than C2 as illustrated. Products will, however, be the same.

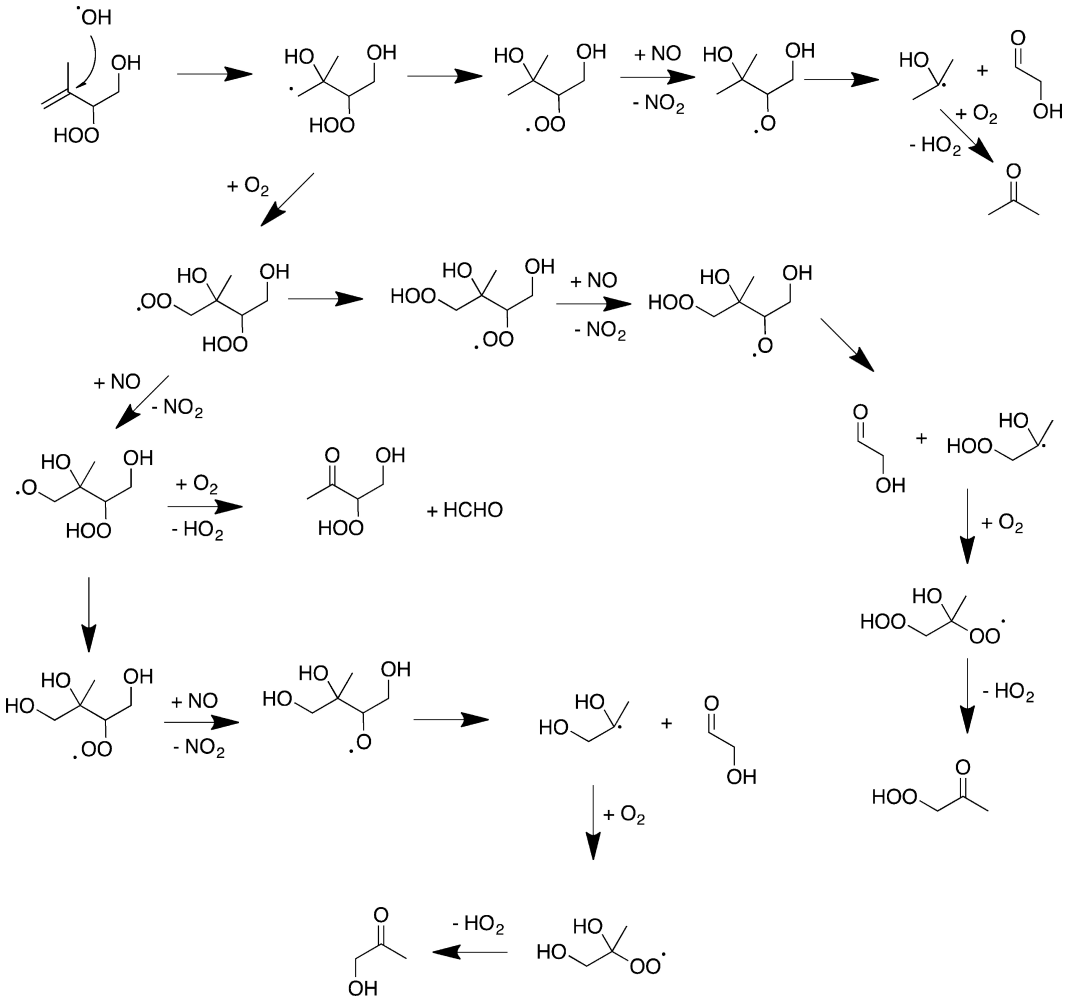

Figure D.8: Internal OH addition mechanism for (4,3)-ISOPOOH under high [NO].

the main sample impurity, the methylbutenediols described above. Synthesized methylbutenediol standards were oxidized in separate experiments under similar conditions to provide a correction factor that was then applied to the ISOPOOH experiments. The correction term was <1% yield for K8 and K9, and ~4% yield for K6. The mean glycolaldehyde yield from the high NO experiments is 14 ± 2%, and was accompanied by a hydroxyacetone yield of 13 ± 2%.

Internal addition to (4,3)-ISOPOOH is expected to be only a small fraction of the reactivity (probably equal to or less than 10% of the external addition). Thus, only a small fraction of the glycolaldehyde yield arises from this channel (Figure D.8). Because of the fast H-shift chemistry between peroxy radicals (Jørgensen *et al.*, 2016), however, this channel may be responsible for the small yield (~2%) of a three carbon hydroperoxy ketone (CF_3O^- cluster *m/z* = 175).

The total (4,3)-ISOPOOH reactivity that yields products other than IEPOX is thus 14% from OH addition and 7% from the sum of all hydrogen abstraction channels. By difference, the IEPOX yield is estimated to be 79%.

The relative amount of *cis*- and *trans*-β-IEPOX was determined using GC-ToF CIMS. The large ISOPOOH peak was removed by scaling the preoxidation chromatogram to match the height of the postoxidation ISOPOOH peak (Figures D.9 and D.10). IEPOX peaks were then fit using Gaussian curves, and the peak areas were scaled by their relative CIMS sensitivities (Bates *et al.*, 2014). The IEPOX yield was determined to be 68 ± 2% *trans*- and 32 ± 2% *cis*-β-IEPOX, assuming equal GC transmission for the two isomers and using our estimate of the relative sensitivity of the CIMS instrument to these two isomers (Bates *et al.*, 2014; Paulot *et al.*, 2009b). Without a direct measurement of the sensitivity, however, the uncertainty in the relative yields is substantially higher (70 ± 20% *trans* and 30 ± 10% *cis*).

D.3.3 Products of OH Addition to (1,2)-ISOPOOH

As was done for the (4,3)-ISOPOOH, the fraction of (1,2)-ISOPOOH that does not form IEPOX following OH addition was determined from the high NO experiments. For (1,2)-ISOPOOH, external OH addition and subsequent O_2 addition in the presence of high NO is expected to produce glycolaldehyde and hydroxyacetone as the major products (Figure D.11). For internal addition of OH (Figure D.12), production of hydroxyacetone can also be accompanied by a two-carbon hydroperoxyaldehyde (CF_3O^- cluster *m/z* = 161) *via* fast H-shift between RO_2 groups. In

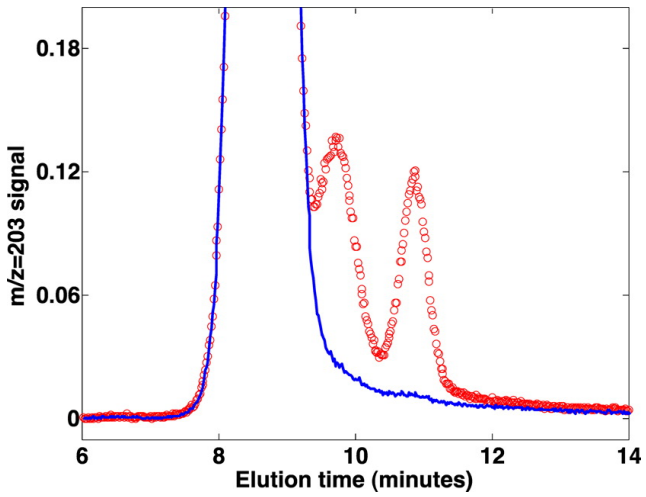

Figure D.9: Removal of the preoxidation (4,3)-ISOPOOH peak (blue line) from the postoxidation m/z = 203 GC-ToF CIMS chromatogram (red circles).

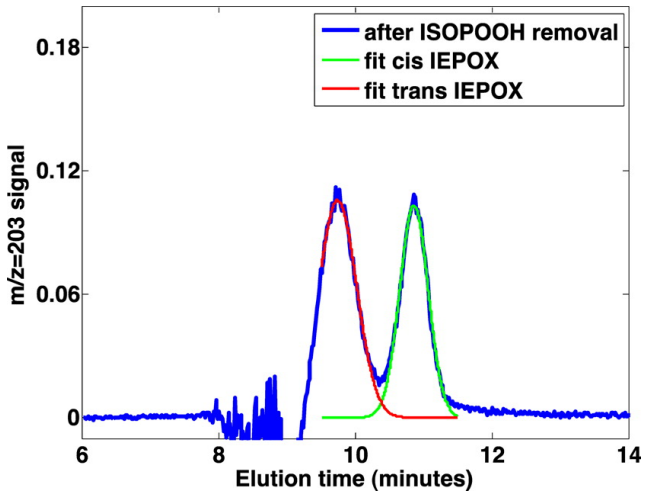

Figure D.10: Fitting the *trans*- and *cis*-β-IEPOX GC-ToF CIMS peaks after ISOPOOH removal. Because of its much higher dipole moment, the CIMS instrument is much more sensitive to the *cis* isomer.

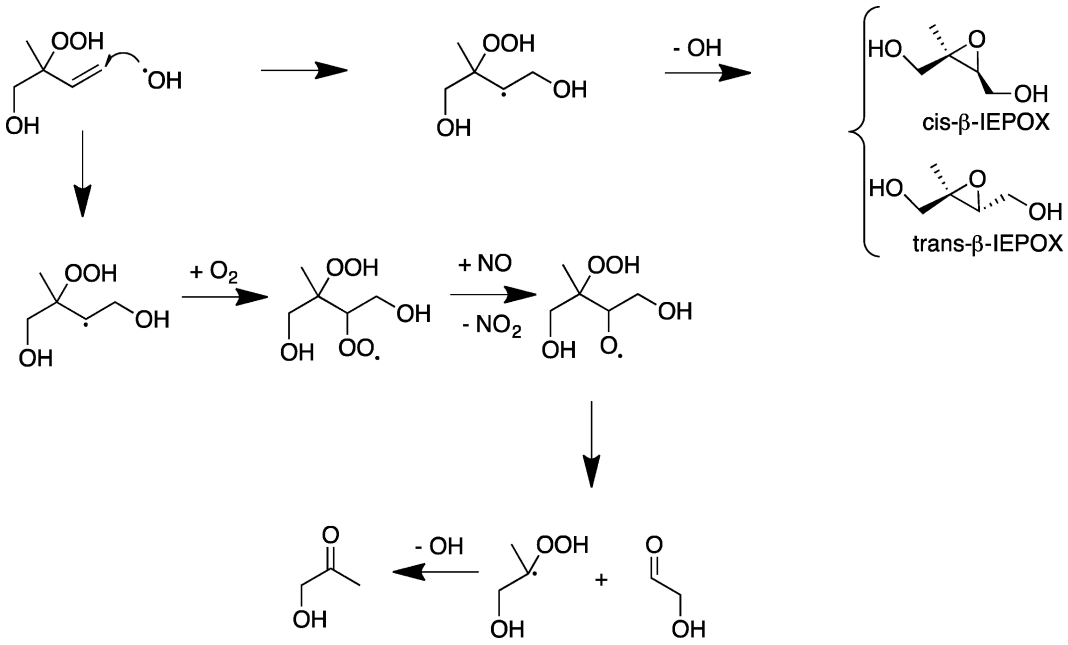

Figure D.11: External OH addition mechanism for (1,2)-ISOPOOH under high [NO]. Owing to the fast H-shift between RO_2 groups, the peroxy radical that reacts with NO may be on C2 rather than C4 as illustrated. Products will, however, be the same.

addition, a small yield of the five carbon dihydroxy hydroperoxy nitrate is expected for both the internal and external OH addition, followed by O_2 addition and NO reaction. From experiments K3, K4, K5, and K7, the hydroxyacetone yield is estimated to be 13 ± 2%. The glycolaldehyde yield is 9 ± 1%. The two-carbon hydroperoxyaldehyde yield is 3 ± 1%. As was done for (4,3)-ISOPOOH, the glycolaldehyde and hydroxyacetone yields were corrected for production from the main sample impurity (no larger than 1% yield correction for all experiments).

By adding the high NO hydroxyacetone yield (13%) to the hydrogen abstraction fraction (16%) we infer (by difference from unity) an IEPOX yield of 71% for the OH oxidation of (1,2)-ISOPOOH. The relative distribution of the two β-IEPOX was determined to be 67 ± 1% *trans* and 33 ± 1% *cis*-IEPOX using GC-ToF CIMS chromatography. The uncertainty is the standard deviation of the measurements and does not include uncertainty in the relative transmission or in the relative sensitivity of the two isomers.

Under low NO conditions, a larger number of products were observed from the oxidation of (1,2)-ISOPOOH than from (4,3)-ISOPOOH. Other than IEPOX, however, no observed product exceeded a 4% yield, and the sum of all observed products

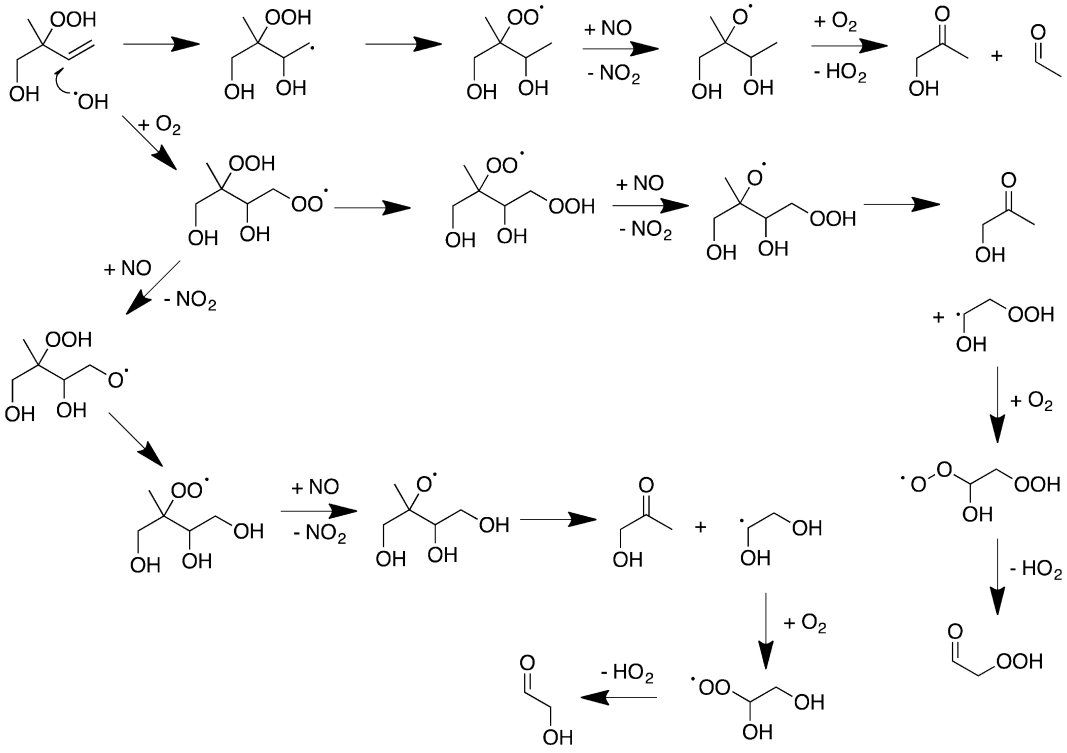

Figure D.12: Internal OH addition mechanism for (1,2)-ISOPOOH under high [NO].

equaled 12% of the ISOPOOH reacted (Table D.5). As with the (4,3)-ISOPOOH, some of the observed products are likely oxidation products of impurities. Tentatively, the *m/z* = 201 (HPALD) is thought to arise from H-abstraction α to the hydroxy, as is *m/z* = 185 (unsaturated epoxide).

Consistent with the observed formation of the C_2 hydroperoxy aldehyde in the high NO experiments, the internal OH addition to (1,2)-ISOPOOH is non-negligible. Under low NO conditions, however, this channel (as well as any non-IEPOX chemistry following addition at C4) likely forms low volatility substituted hydroperoxide products that are lost to the chamber walls and sample tubing. One likely product, a dihydroperoxydiol, would be observed at *m/z* = 253. Alternatively, ketones or aldehydes produced *via* autoxidation of the RO_2 may form. Because of either uptake on the chamber walls or fragmentation in the CF_3O^- ionization, no signal at the expected *m/z* was observed.

D.3.4 Ab Initio Calculations

Both (1,2)-ISOPOOH + OH and (4,3)-ISOPOOH + OH reactions were investigated using ab initio techniques, with the details contained in the Supporting Infor-

pathway	(4,3)-ISOPOOH	(1,2)-ISOPOOH
cis-β-IEPOX	40.1	26.7
trans-β-IEPOX	46.7	19.0
external OH, O_2 addition	8.3	10.2
internal OH, O_2 addition	1.2	29.0
OOH H-abstraction	0.9	7.2
OH H-abstraction	0.0	1.4
CH_2 H-abstraction	0.2	6.5
CH H- abstraction	2.6	N/A

Table D.7: Reaction pathway yields (%) calculated with MESMER modeling.

mation and a brief summary given here. The reactions were assumed to proceed *via* a reactive complex ISOPOOH-OH before forming a transition state and yielding the different products. The energies of the numerous structures between and including the reactants and products were calculated relative to the starting ISOPOOH + OH energy. All calculations were performed using the Gaussian 09 suite (Frisch *et al.*, 2009) with the M06-2X/aug-cc-pVTZ method (Knap *et al.*, 2015). The kinetic rate calculations were carried out using the Master Equation Solver for Multi Energy well Reaction (MESMER) (Glowacki *et al.*, 2012). The Arrhenius pre-exponential factors (A) used in MESMER were selected to best match the experimental overall addition and H- abstraction reaction rate constants for each ISOPOOH isomer. Calculated individual rate constants for each reaction channel provide estimates of product yields, including the IEPOX isomer (*cis* vs *trans*) and the dihydroperoxy diol from O_2 addition.

D.3.5 (4,3)-ISOPOOH

An abstraction rate constant of 7.2×10^{-12} cm^3 molecule^{-1} s^{-1} and an addition rate constant of 9.7×10^{-11} cm^3 molecule^{-1} s^{-1} were determined assuming A = 5.0×10^{-12} cm^3 molecule^{-1} s^{-1} and 1.5×10^{-10} cm^3 molecule^{-1} s^{-1}, for these channels, respectively. The reaction pathway yields are summarized in Table D.7.

External OH addition dominated, with 95% of the total yield, and 87% of the total yield forming IEPOX. The IEPOX yield is similar to the experimental yield, and the *trans* isomer fraction at 54% is slightly below the experimental value of 68 ± 2% but with the same preference for formation of the *trans* isomer. The O_2 addition channels from internal and external addition are calculated to be ∼10%, within the uncertainty of the experimental estimate (13 ± 4%). The hydroperoxy

hydrogen abstraction was calculated as ~1%, which is smaller than the experimental value (4%).

D.3.6 (1,2)-ISOPOOH

An abstraction rate constant of 1.2×10^{-11} cm^3 molecule^{-1} s^{-1} and an addition rate constant of 6.2×10^{-11} cm^3 molecule^{-1} s^{-1} were determined by using A = 1×10^{-11} cm^3 molecule^{-1} s^{-1} and 6×10^{-11} cm^3 molecule^{-1} s^{-1}, for these channels, respectively. The reaction pathway yields are summarized in Table D.7. The abstraction reactions account for 15% (with 7% attributed to abstraction of the hydroperoxy hydrogen) compared to 12% from the experimental data. The addition channels exhibit a bigger difference between the calculated and experimental yields. The calculated yield of IEPOX is 46%. Following either internal or external OH addition, 39% proceeds *via* O_2 addition. Assuming that O_2 addition ultimately yields hydroxyacetone under high NO conditions, the experimental data suggest the O_2 addition channels account for less than half of the calculated yield. The IEPOX isomer yield is notably different for the calculations compared to the experimental data: in the calculations, the *cis* isomer is preferred (58% of total IEPOX) while the experimental results suggest the *trans* isomer is preferred at 67 ± 1% of the total IEPOX.

D.3.7 Atmospheric Implications

The global impact of recent changes to the HO_2-dominated pathway of the isoprene oxidation mechanism were investigated using the GEOS-Chem chemical transport model (Bey *et al.*, 2001). Three sets of simulations were run for the year 2012 with a model spin-up of 1.5 years. All three simulations employed version 9.02 of GEOS-Chem on a 4×5 degree grid, with GEOS5 meteorology and the Rosenbrock Rodas-3 solver.

The first simulation used the isoprene mechanism in the current GEOS-Chem version (v9-02) (Mao *et al.*, 2013), hereafter referred to as "Standard". The second simulation, denoted "Old", restored the HO_2-dominated pathway of the isoprene oxidation mechanism to that of Paulot *et al.* (2009b) The "Standard" and "Old" simulations differed only in their ISOPOOH H-abstraction rate constant and ISOPOO recycling yield, and in their HO_2 + RO_2 rate constant: the "Standard" used k = $2.91 \times 10^{-13} \times e^{(1300/T)} \times [1 - e^{(-0.245 \times n)}]$ (Jenkin *et al.*, 1997; Saunders *et al.*, 2003) and the "Old" used k = $7.4 \times 10^{-13} \times e^{(700/T)}$ (Paulot *et al.*, 2009b). The third simulation updated the mechanism with the results from this study and that of Bates *et al.* (2014)

mechanisms:	old[a]	standard	recommended
ISOPOOH produced (Tg C/y)	129	168	181
IEPOX produced (Tg C/y)	94	122	115

[a] Paulot *et al.* (2009b)

Table D.8: Yearly ISOPOOH and IEPOX production for three GEOS-Chem simulations with differing isoprene oxidation mechanisms. Global isoprene emissions are 454 Tg C each year in all simulations

as well as an ISOPOOH yield of 94% from HO_2 + ISOPOO (Liu *et al.*, 2013) and a speciated ISOPOOH and IEPOX distribution to utilize the isomer-specific reaction rate constants and product yields (see Supporting Information). The third simulation is referred to as "Recommended".

The increase in the $HO_2 + RO_2$ rate constant had the largest effect on the ISOPOOH and IEPOX produced, with the annual production of both species 30% higher in the "Standard" run than the "Old" run (Table D.8). From the "Standard" to the "Recommended" simulation, the ISOPOOH yield from $HO_2 + RO_2$ increased but so did the ISOPOOH + OH rate constant, resulting in a net 8% increase in ISOPOOH. Despite a lower OH + IEPOX rate constant, the IEPOX decreased by 9% due to the lower IEPOX yield from the OH addition to ISOPOOH in the "Recommended" simulation.

isoprene emissions for all simulations were 454 Tg C y^{-1}, resulting in 115 Tg C y^{-1} of IEPOX in the "Recommended" run, about 20 Tg C y^{-1} higher than in the "Old" simulation. The global average distribution for IEPOX in the "Recommended" simulation is shown in Figure D.13 for northern hemisphere summer (JJA) and winter (DJF). The highest IEPOX concentrations for both seasons appear in the Southern Hemisphere (South America and Africa), though in the Northern Hemisphere summer significant IEPOX is produced in the Southeastern United States and in the boreal forests.

D.3.8 isoprene Hydroxynitrates as an IEPOX Source

Two recent laboratory studies have demonstrated a path to IEPOX formation from oxidation of isoprene by OH under NO-dominated conditions, *via* OH addition to isoprene hydroxynitrates (ISOPN) (Jacobs *et al.*, 2014; Lee *et al.*, 2014). Data from both studies are consistent with an IEPOX yield of 12-13% from the (4,3)-ISOPN. From the experiments described by Lee *et al.* (2014) we estimate the combined

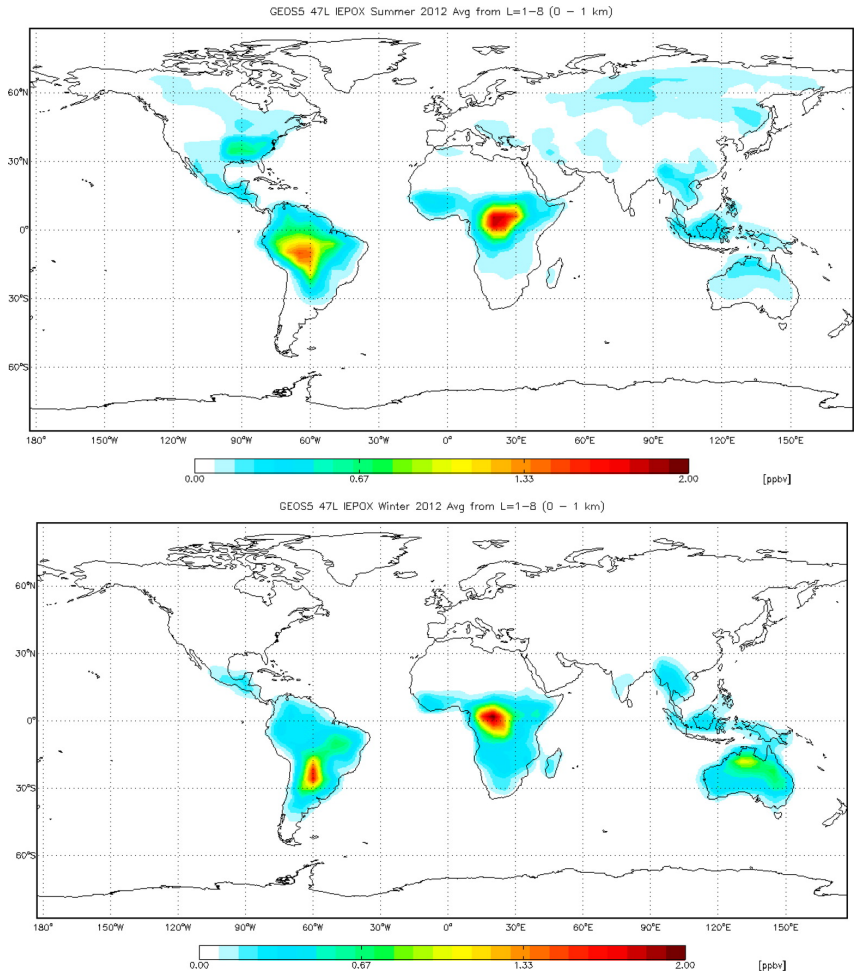

Figure D.13: Average distribution for IEPOX during northern hemisphere summer (top) and winter (bottom) using GEOS-Chem with an updated isoprene mechanism.

yield of IEPOX from the two β ISOPN to be 15 ± 3%. To evaluate the atmospheric importance of this channel to the global IEPOX budget, an upper limit IEPOX yield of 18% was implemented for a GEOS-Chem simulation with all other input identical to the "Recommended" simulation. The global IEPOX production changed from 115 to 116 Tg C y^{-1}, suggesting that the ISOPN channel contributes only ~1% to the total IEPOX production.

D.3.9 Formation of Low Volatility Compounds Other than IEPOX

Following addition of OH to ISOPOOH, our experiments suggest that a number of low volatile products including dihydroperoxydiols, aldehydes, and ketones will form in low NO environments. Assuming these channels together account for ~15% of the products of the OH addition to ISOPOOH, approximately 20 Tg C of low

volatility hydroperoxide compounds are formed each year globally. While these compounds will likely add to the organic aerosol burden, their lifetimes may be short due to photolysis and subsequent fragmentation. Recent laboratory and field observations (Krechmer *et al.*, 2015; Nguyen *et al.*, 2014b) provide evidence for the importance of this chemistry and suggest further study to place the atmospheric mechanistic pathways involved on a more firm footing.

D.4 Conclusions

The photochemistry of ISOPOOH is central to the oxidation of isoprene under HO_2-dominated conditions. Synthetic standards of the two major ISOPOOH isomers, (1,2)-ISOPOOH and (4,3)-ISOPOOH, enabled the direct and isomer-specific measurement of ISOPOOH + OH product yields and reaction rate constants relative to propene. The isomer-averaged OH addition rate coefficient was similar to a previous estimate while the H-abstraction rate coefficient was faster (Paulot *et al.*, 2009b). The rate constants for OH reaction with the two ISOPOOH are sufficiently different that the overall ISOPOOH loss rate to OH will be affected by the relative production rates of the ISOPOOH isomers, which in turn are determined by the isoprene RO_2 distribution.

IEPOX is the major product of this chemistry. The *cis*- and *trans*-β-IEPOX relative product distribution was similar from the two ISOPOOH isomers and was also similar to the previous estimate (Bates *et al.*, 2014). The total IEPOX yield, however, was estimated to differ somewhat between the two ISOPOOH due to the larger importance of internal OH addition to the (1,2)-ISOPOOH.

Because the two IEPOX isomers differ in their OH reaction rates, the unequal isomer distribution affects the overall IEPOX loss rate to OH reaction, with the observed distribution reacting 8% slower than an equal distribution (Bates *et al.*, 2014). Organic aerosol formation studies with synthesized IEPOX standards suggest little or no difference in aerosol formation between the two IEPOX isomers (Nguyen *et al.*, 2014a). Any difference in aerosol formation between the two isomers in the atmosphere would instead be due to the difference in their OH lifetimes causing more *trans*-β-IEPOX to be available for uptake.

Finally, a non-negligible fraction of the ISOPOOH oxidation likely leads to the formation of highly oxidized five carbon peroxy radicals. Under low NO or long RO_2 lifetimes, these channels will likely yield very low vapor pressure compounds that contribute to aerosol formation.

D.5 Supporting Information

D.5.1 CIMS Sensitivities

CIMS sensitivities to the oxidation products were determined in multiple ways. Hydroxyacetone and glycolaldehyde are commercially available and were quantified gravimetrically and by Fourier transform Infrared Spectroscopy (FT-IR) for CIMS calibration (St. Clair *et al.*, 2014). Uncalibrated compounds (glycolic acid and all products identified by *m/z*) were assigned a generic CIMS sensitivity of 2.5×10^{-4} ncts /pptv, and are considered accurate to within a factor of 2. Here, normalized counts (ncts) represent the counts observed at the analyte *m/z* divided by the reagent ion counts. The reagent ion counts are the sum of the signal at *m/z* = 86 ($^{13}CF_3O^-$) and *m/z* = 104 ($^{13}CF_3O^-\cdot H_2O$), as well as *m/z* = 120 ($^{13}CF_3O^-\cdot H_2O_2$) for experiments with H_2O_2 as the OH source.

The sensitivities for ISOPOOH and IEPOX were obtained by matching the output of a box model to a laboratory isoprene + OH oxidation under low NO conditions. The sensitivity is therefore dependent on the box model chemistry, including the yield of ISOPOOH from isoprene (0.94) and the yield of IEPOX from ISOPOOH (0.8). The ISOPOOH yield used was based on a 6% yield of methyl vinyl ketone and methacrolein (Liu *et al.*, 2013), and the IEPOX yield used was 80%, in general agreement with the sum of the nonIEPOX products observed by the CIMS in this study. ToF-CIMS sensitivities for ISOPOOH and IEPOX were 1.6×10^{-4} ncts pptv^{-1} and 1.9×10^{-4} ncts pptv^{-1}, respectively. For the TQ-CIMS, the MSMS sensitivities were 5.1×10^{-6} ncts pptv^{-1} and 3.9×10^{-6} ncts pptv^{-1} for ISOPOOH and IEPOX, respectively. The CIMS sensitivity to ISOPOOH was also verified gravimetrically by completely evaporating a known mass of the pure compound into a known volume of dry air. For the (4,3)-ISOPOOH, the sample evaporated completely and gave a sensitivity of 1.6×10^{-4} ncts pptv^{-1}. The (1,2)-ISOPOOH gave a sensitivity of 1.5×10^{-4} ncts pptv^{-1} but with a slight residual mass, and 1.6×10^{-4} ncts pptv^{-1} was determined appropriate for both isomers.

D.5.2 Impurity Oxidation Products

The main impurities in the ISOPOOH samples, 2-methyl-1-butene-3,4-diol for (4,3)-ISOPOOH and 3-methyl-1-butene-3,4-diol for (1,2)-ISOPOOH, also react with OH to produce some of the same product masses as ISOPOOH. To correct for the impurity oxidation products, both methylbutanediols were synthesized and each was oxidized by OH under similar conditions to the ISOPOOH experiments. The ratio of the product formation to methylbutanediol loss was then used to remove

the methylbutanediol products from the ISOPOOH experiment data.

D.5.3 Ab Initio Calculations

We used the M06-2X/aug-cc-pVTZ method as implemented in the Gaussian 09 program (Frisch *et al.*, 2009). Frequency calculations were done at all stationary points with the same method to ensure that the equilibrium structures (reactants, reactive complexes, products) only have positive vibrational frequencies and the transition states have one imaginary frequency. To ensure that the transition state connects the reactive complex and the product, intrinsic reaction coordinate (IRC) calculations were performed and, if needed, the end product was optimized (Gonzalez and Schlegel, 1989, 1990). None of the M06-2X/aug-ccpVTZ calculations have any significant spin contamination. Single point energy CCSD(T)-F12a/VDZ-F12 [F12] calculations were performed on the M06-2X/aug-ccpVTZ geometries (Adler *et al.*, 2007; Peterson *et al.*, 2008). All the CCSD(T) calculations were carried out with the Molpro2012 program suite using default convergence criteria (Werner *et al.*, 2012). High T1-diagnostic values were observed for H-abstraction from the OH group, and we have therefore used the M06-2X/aug-cc-pVTZ energies for Mesmer modeling. High T1-diagnostic values have been observed previously for H-shift from OH groups (Knap *et al.*, 2015; Peeters and Nguyen, 2012). For OH addition and H-abstraction involving -CH_2 and >CH groups, the M06-2X/aug-cc-pVTZ energies of the reactant complex and the transition state are in good agreement with the CCSD(T)-F12A/VDZF12 energies. The M06-2X/aug-cc-pVTZ (and wb97-XD) method has also previously been found to calculate barrier heights similar to those obtained with the much more computationally expensive CCSD(T)-F12A/VD2-F12 single point calculations on the DFT geometry (Knap *et al.*, 2015). In the following we are therefore using the M06-2X/aug-cc-pVTZ energies for kinetic modeling.

D.5.3.1 The energetics of the reaction between ISOPOOH and OH

We have assumed that the association reaction between OH and ISOPOOH produces a reactive complex (ISOPOOH-OH). The reactive complex can hereafter overcome the transition state and produce the different product complexes and products.

OH + ISOPOOH → ISOPOOH-OH → Products

In Figures D.14 and D.15 the different reaction pathways for (1,2)-ISOPOOH and (4,3)-ISOPOOH are shown, respectively, and the energetics of the reaction pathways are given in Tables D.9 and D.10. The reactant complexes for each of the individual

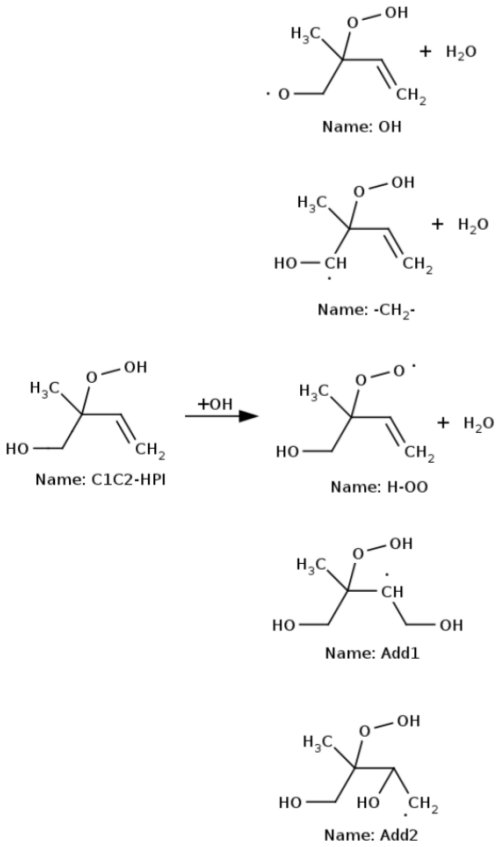

Figure D.14: The different reaction pathways for the reaction between (1,2)-ISOPOOH and the OH radical.

reaction paths are different.

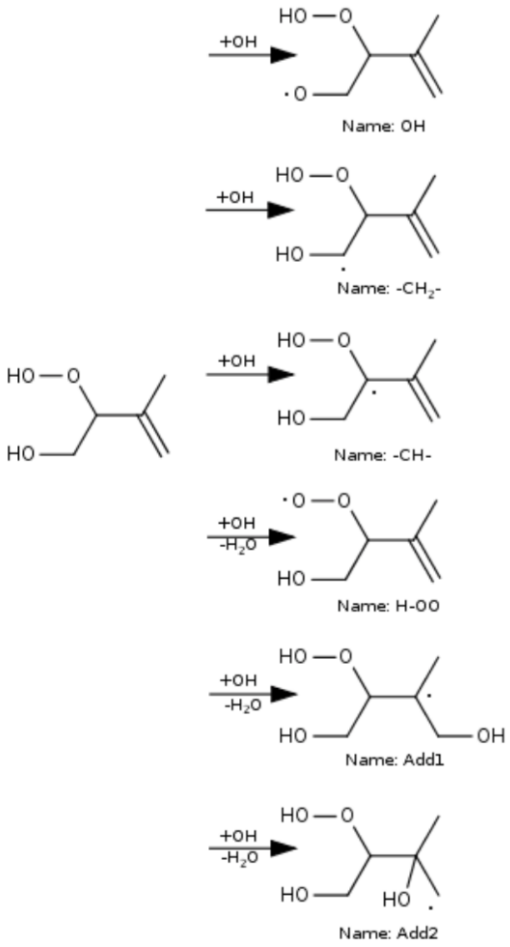

Figure D.15: The different reaction pathways for the reaction between (4,3)-ISOPOOH and the OH radical.

	OH	-CH_2-	H-OO	Add1	Add2
(1,2)-ISOPOOH+OH	0.0	0.0	0.0	0.0	0.0
Reactive Complex	-8.9 (-8.3)	-7.3 (-6.1)	-5.0 (-3.7)	-6.2 (-6.1)	-7.8 (-6.2)
Transition State	-2.2 (-1.0[a])	-4.0 (-3.5)	-3.8 (-3.3)	-5.3 (-5.2)	-5.6 (-5.4)
Product Complex	-21.8 (-20.9)	-34.0 (-33.0)	-40.8 (-40.2)	-	-
Product	-13.8 (-8.7)	-24.2 (-23.5)	-34.7 (-34.4)	-34.4 (-31.1)	-33.4 (-30.0)

Table D.9: The relative energies (kcal mol^{-1}) for the reaction between the (1,2)-ISOPOOH molecule and the OH radical with the M06-2X/aug-cc-pVTZ method and the F12//M06- 2X/aug-cc-pVTZ. The values in () are the F12//M06-2X/aug-cc-pVTZ values. The energies are corrected with zero point vibrational energies. The marked calculation ([a]) has a T1 diagnostic value of 0.078.

	OH	-CH_2-	-CH-	H-OO	Add1	Add2
(4,3)-ISOPOOH+OH	0.0	0.0	0.0	0.0	0.0	0.0
Reactive Complex	-6.2 (-5.3)	-6.8 (-6.2)	-6.4 (-4.9)	-5.7 (-4.4)	-7.7 (-6.5)	-5.8 (-4.3)
Transition State	-0.4 (25.6[a])	-1.7 (-1.3)	-4.8 (-4.5)	-2.8 (-1.5[b])	-7.7 (-7.0)	-2.7 (-5.1)
Product Complex	-19.4 (-18.1)	-30.6 (-29.2)	-43.0 (-41.3)	-36.0 (-35.1)	-	-
Product	-10.8 (-9.7)	-23.2 (-22.5)	-33.9 (-34.2)	-33.4 (-33.2)	-34.9 (-31.7)	-31.2 (-28.7)

Table D.10: The relative energies (kcal mol^{-1}) for the reaction between (4,3)-ISOPOOH and OH with the M06-2X/aug-cc-pVTZ method and the F12//M06-2X/aug-cc-pVTZ. The values in () are the F12//M06-2X/aug-cc-pVTZ values.. The energies are corrected with zero point vibrational energies. Marked calculations have T1 diagnostic values of [a]0.116 and [b]0.058.

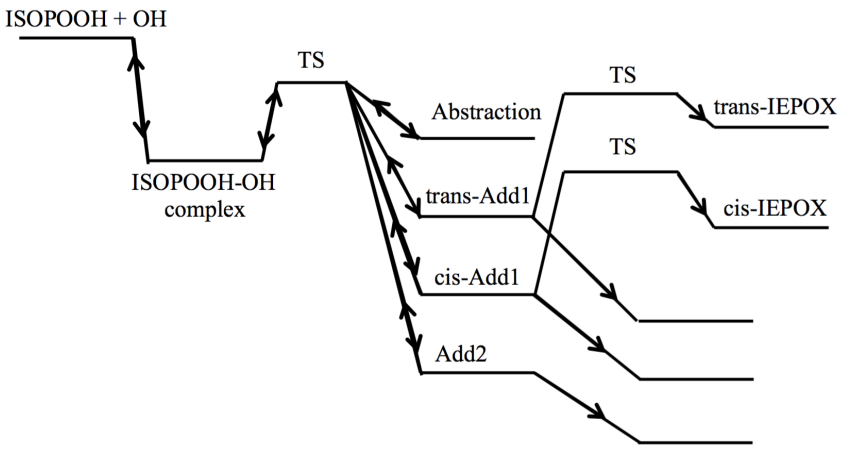

Figure D.16: The reaction scheme as used in the MESMER model (Only an illustration, not the energetically correct picture of the reactions). The ISOPOOH-OH complexes are different for each of the reaction pathways even though they are given with the same energy at this figure.

D.5.3.2 The kinetics of the reaction between ISOPOOH and OH

The kinetic calculations are carried out using the master equation solver for multi energy well reaction, MESMER program (Glowacki *et al.*, 2012). The general reaction scheme is shown in Figure D.16.

In our Mesmer modeling the Lennard-Jones (L-J) parameters of the bath gas were chosen to be a nitrogen gas resembling the atmospheric gas (σ (N_2) = 3.919 Å, ϵ/k_b (N_2) = 91.85 K) whereas the reactive complex (ISOPOOH-OH) is modeled with the L-J parameters of methylcyclohexane (σ (methylcyclohexane) = 7.045 Å, ϵ/k_b (methylcyclohexane) = 379.95 K) (Cuadros *et al.*, 1996). The average collisional activation/deactivation energy transfer of all the molecules is set to 200 cm^{-1} per collision and the grain size of each grain is 50 cm^{-1}. The span of the energy grains is set to 30 kT above the highest stationary point. We have used a pressure of 745 Torr and a temperature of 298 K for all the calculations, similar to the experimental conditions.

We have performed a sensitivity test of Mesmer input parameters. In our sensitivity test we used three collisional activation/deactivation energies of 50, 100 and 200 cm^{-1} and two different grain sizes of 25 and 50 cm^{-1}. We did not observe any significant changes in the reaction rate constants (only changes of a few percent). We have also tested the system with different sizes of grain span, *e.g.*, 10 kT, 20 kT, 30 kT, 40 kT, and 50 kT. If a grain span of 30 kT or higher is used, the reaction rate

constants do not change. We have therefore used a grain size of 30 kT.

The reaction rate constants are sensitive to the choice of the Arrhenius pre-exponential factor (A). Each reaction pathway is a separate Mesmer calculation (See Figures D.17 and D.18 for the individual reaction pathways) – we have not coupled between the reactions in the fitting of the Arrhenius pre-exponential factor (A). We treat the pre-exponential factor as temperature independent and it is varied between 1.0×10^{-12} and 2.0×10^{-10} cm^3 $molecule^{-1}$ s^{-1}. We use nine different Arrhenius pre-exponential factors to calculate the rates. Three of the factors are from the three reactions of n-butane, 3-methyl-3-butene-1-ol and 1-butene with OH (Atkinson and Arey, 2003a; Cometto *et al.*, 2008; Vakhtin *et al.*, 2003). The total reaction rate constants (OH +ISOPOOH $\rightarrow$ Products) of the (1,2)-ISOPOOH and (4,3)-ISOPOOH systems are shown in Table D.11 and Table D.12, respectively.

reaction	A($1\cdot10^{-12}$)[a]	A($2\cdot10^{-12}$)	A($5\cdot10^{-12}$)[b]	A($1\cdot10^{-11}$)	A($3\cdot10^{-11}$)[c]	A($6\cdot10^{-11}$)	A($1\cdot10^{-10}$)	A($1.5\cdot10^{-10}$)	A($2\cdot10^{-10}$)	Mix
OH	$3.3\cdot10^{-13}$ (8.3)	$4.7\cdot10^{-13}$ (6.4)	$6.8\cdot10^{-13}$ (4.2)	$8.2\cdot10^{-13}$ (3.0)	$1.0\cdot10^{-12}$ (1.7)	$1.1\cdot10^{-12}$ (1.2)	$1.2\cdot10^{-12}$ (1.0)	$1.2\cdot10^{-12}$ (0.8)	$1.2\cdot10^{-12}$ (0.8)	$8.2\cdot10^{-13}$ (1.1)
-CH_2-	$8.6\cdot10^{-13}$ (21.8)	$1.6\cdot10^{-12}$ (21.4)	$3.2\cdot10^{-12}$ (20.2)	$5.2\cdot10^{-12}$ (18.7)	$9.2\cdot10^{-12}$ (15.5)	$1.2\cdot10^{-11}$ (13.5)	$1.4\cdot10^{-11}$ (12.1)	$1.6\cdot10^{-11}$ (11.0)	$1.7\cdot10^{-11}$ (10.4)	$5.2\cdot10^{-12}$ (7.0)
H-OO	$9.0\cdot10^{-13}$ (22.8)	$1.7\cdot10^{-12}$ (22.8)	$3.6\cdot10^{-12}$ (22.3)	$5.8\cdot10^{-12}$ (21.2)	$1.1\cdot10^{-11}$ (18.3)	$1.4\cdot10^{-11}$ (16.1)	$1.7\cdot10^{-11}$ (14.3)	$1.9\cdot10^{-11}$ (13.2)	$2.0\cdot10^{-11}$ (12.4)	$5.8\cdot10^{-12}$ (7.9)
Add1 (C1)	$9.8\cdot10^{-13}$ (24.9)	$1.9\cdot10^{-12}$ (26.3)	$4.7\cdot10^{-12}$ (29.3)	$9.0\cdot10^{-12}$ (32.6)	$2.3\cdot10^{-11}$ (39.4)	$4.0\cdot10^{-11}$ (44.3)	$5.6\cdot10^{-11}$ (48.0)	$7.2\cdot10^{-11}$ (50.6)	$8.5\cdot10^{-11}$ (52.4)	$4.0\cdot10^{-11}$ (53.7)
Add2 (C2)	$8.8\cdot10^{-13}$ (22.3)	$1.7\cdot10^{-12}$ (23.0)	$3.8\cdot10^{-12}$ (24.0)	$6.8\cdot10^{-12}$ (24.6)	$1.5\cdot10^{-11}$ (25.1)	$2.2\cdot10^{-11}$ (24.9)	$2.9\cdot10^{-11}$ (24.6)	$3.5\cdot10^{-11}$ (24.3)	$3.9\cdot10^{-11}$ (24.0)	$2.2\cdot10^{-11}$ (30.2)

Table D.11: The reaction rate constants at 298K (in cm^3 $molecules^{-1}$ s^{-1}) for the reaction between the (1,2)-ISOPOOH molecule and the OH radical with the M06-2X/aug-cc-pVTZ method. All the reaction rates are without tunneling correction. In () are the yields in percent. The ratios are calculated as Γ_i=k_i/k_{tot} ×100%, where $k_{tot} = \Sigma k_i$. In the Mix column, the addition and the abstraction reactions use an Arrhenius value of $6\cdot10^{-11}$ and $1\cdot10^{-11}$ cm^3 $molecule^{-1}$ s^{-1}, respectively. Marked preexponential factors are from [a]an OH reaction with n-butane (Abstraction) [3], [b] the reaction of OH with 3-methyl-3-buten-1-ol (Addition and Abstraction)[4], and [c]OH and 1-butene (Addition)[5].

reaction	A($1\cdot10^{-12}$)[a]	A($2\cdot10^{-12}$)	A($5\cdot10^{-12}$)[b]	A($1\cdot10^{-11}$)	A($3\cdot10^{-11}$)[c]	A($6\cdot10^{-11}$)	A($1\cdot10^{-10}$)	A($1.5\cdot10^{-10}$)	A($2\cdot10^{-10}$)	Mix
OH	7.1·10-14 (1.2)	7.7·10-14 (1.2)	8.1·10-14 (0.6)	8.2·10-14 (0.4)	8.4·10-14 (0.2)	8.5·10-14 (0.1)	8.5·10-14 (0.1)	8.5·10-14 (0.1)	8.5·10-14 (0.0)	8.1·10-14 (0.1)
-CH_2-	$3.1\cdot10^{-13}$ (6.8)	$4.2\cdot10^{-13}$ (6.8)	$5.5\cdot10^{-13}$ (4.4)	$6.3\cdot10^{-13}$ (3.0)	$7.2\cdot10^{-13}$ (1.6)	$7.7\cdot10^{-13}$ (1.0)	$7.9\cdot10^{-13}$ (0.7)	$8.0\cdot10^{-13}$ (0.6)	$8.1\cdot10^{-13}$ (0.5)	$5.5\cdot10^{-13}$ (0.5)
-CH-	$9.3\cdot10^{-13}$ (29.3)	$1.8\cdot10^{-12}$ (29.3)	$4.1\cdot10^{-12}$ (33.3)	$7.4\cdot10^{-12}$ (35.7)	$1.7\cdot10^{-11}$ (36.3)	$2.5\cdot10^{-11}$ (33.6)	$3.2\cdot10^{-11}$ (30.3)	$3.9\cdot10^{-11}$ (27.2)	$4.4\cdot10^{-11}$ (24.9)	$4.1\cdot10^{-12}$ (4.0)
H-OO	$7.9\cdot10^{-13}$ (21.8)	$1.3\cdot10^{-12}$ (21.8)	$2.4\cdot10^{-12}$ (19.1)	$3.3\cdot10^{-12}$ (15.9)	$4.8\cdot10^{-12}$ (10.5)	$5.5\cdot10^{-12}$ (7.4)	$6.0\cdot10^{-12}$ (5.6)	$6.3\cdot10^{-12}$ (4.4)	$6.5\cdot10^{-12}$ (3.7)	$2.4\cdot10^{-12}$ (2.3)
Add1 (C1)	$6.9\cdot10^{-13}$ (22.3)	$1.4\cdot10^{-12}$ (22.3)	$3.4\cdot10^{-12}$ (27.4)	$6.8\cdot10^{-12}$ (32.7)	$2.0\cdot10^{-11}$ (44.0)	$3.9\cdot10^{-11}$ (52.7)	$6.4\cdot10^{-11}$ (59.4)	$9.2\cdot10^{-11}$ (64.7)	$1.2\cdot10^{-10}$ (68.3)	$9.2\cdot10^{-11}$ (89.0)
Add2 (C2)	$7.0\cdot10^{-13}$ (18.5)	$1.1\cdot10^{-12}$ (18.5)	$1.9\cdot10^{-12}$ (15.2)	$2.5\cdot10^{-12}$ (12.1)	$3.4\cdot10^{-12}$ (7.5)	$3.8\cdot10^{-12}$ (5.2)	$4.1\cdot10^{-12}$ (3.8)	$4.3\cdot10^{-12}$ (3.0)	$4.4\cdot10^{-12}$ (2.5)	$4.3\cdot10^{-12}$ (4.1)

Table D.12: The absolute reaction rates at 298K in units of cm^3 $molecules^{-1}$ s^{-1} for the OH radical reaction with the (4,3)-ISOPOOH molecule with the M06-2X/aug-cc-pVTZ method. All the reaction rates are without tunneling correction. In () are the ratios of the different OH and (4,3)-ISOPOOH reactions shown. The ratios are calculated as Γ_i=k_i/k_{tot} ×100%, where $k_{tot} = \Sigma k_i$. In the Mix column, the addition and the abstraction reactions use an Arrhenius value of $1.5\cdot10^{-10}$ and $5\cdot10^{-12}$ cm^3 $molecule^{-1}$ s^{-1}, respectively. Marked preexponential factors are from [a]an OH reaction with n-butane (Abstraction) [3], [b] the reaction of OH with 3-methyl-3-buten-1-ol (Addition and Abstraction)[4], and [c]OH and 1-butene (Addition)[5].

D.5.3.3 (1,2)-ISOPOOH

For the (1,2)-ISOPOOH + OH reactions, the absolute rate constants of all the different reaction pathways increase with an increase in the Arrhenius pre-exponential factor, and the relative yields (in %) of the reaction pathways also change. The yield of the two addition reactions increased more compared to yield of the three abstraction reaction pathways with increasing Arrhenius pre-exponential factor. The rate constant is sensitive to the Arrhenius pre-exponential factor since the energy of the transition state is below the energy of the individual reactants. The rate constant for each reaction path is therefore almost identical to the Arrhenius pre-exponential factor.

With an Arrhenius pre-exponential factor of 1×10^{-11} cm^3 molecule^{-1} s^{-1} for the OH abstraction reactions and 6×10^{-11} cm^3 molecule^{-1} s^{-1} for the addition reactions (see Mix column, Table D.11), the yield of the (1,2)-ISOPOOH + OH reactions is OH (1.1), -CH_2- (7.0), H-OO (7.9), Add1 (53.7), and Add2 (30.2). The rate constant for abstraction is 1.2×10^{-11} cm^3 molecule^{-1} s^{-1} and the rate constant for addition is 6.2×10^{-11} cm^3 molecule^{-1} s^{-1}. The sum of the OH addition and OH abstraction rate constants are 7.4×10^{-11} cm^3 molecule^{-1} s^{-1}, and was constrained to mimic the experimentally determined rate.

D.5.3.4 (4,3)-ISOPOOH

With an Arrhenius pre-exponential factor of 5×10^{-12} cm^3 molecule^{-1} s^{-1} for the OH abstraction reactions and 1.5×10^{-10} cm^3 molecule^{-1} s^{-1} for the addition reactions (see Mix column, Table D.12), the yield of the (4,3)-ISOPOOH + OH reactions is OH (0.1), -CH_2- (0.5), -CH- (4.0), H-OO (2.3), Add1 (89.0), and Add2 (4.1). The rate constant for abstraction is 7.2×10^{-12} cm^3 molecule^{-1} s^{-1} and the rate constant for addition is 9.7×10^{-11} cm^3 molecule^{-1} s^{-1}. The sum of these, 1.1×10^{-10} cm^3 molecule^{-1} s^{-1}, was constrained to mimic the experimentally determined rate.

D.5.3.5 IEPOX production

The formation of *cis*-β-IEPOX (*cis*-C_1C_2), the product of the addition to C1 in (1,2)-ISOPOOH, has a rate constant (the "energetically cold" reaction rate constant) which is three times faster than the rate constant for the formation of *trans*-β-IEPOX (trans-C_1C_2). The *trans*-β-IEPOX (trans-C_4C_3) rate is faster than the *cis*-β-IEPOX (*cis*-C_4C_3) production rate in the (4,3)-ISOPOOH+OH reaction. The *trans*-C_4C_3 rate constant is fastest because of a lower transition state barrier. The differences

Species	ΔE forward / (kcal mol^{-1})	k$_{TST}$ / (s^{-1})	k$_{TST\cdot\kappa_{Eckart}}$ / (s^{-1})
cis-C_1C_2	12.8	3.7×10^3	9.2×10^3
trans-C_1C_2	12.8	1.1×10^3	2.8×10^3
cis-C_4C_3	12.4	2.1×10^3	4.9×10^3
trans-C_4C_3	10.6	3.5×10^4	7.4×10^4

Table D.13: The energy barriers, transition state theory (TST) reaction rate constants and the Eckart-corrected TST reaction rate constants for the production of IEPOX. The energies are calculated with the M06-2X/aug-cc-pVTZ method.

between the reaction rate constants of the *cis*/trans-C_1C_2 isomers are due to changes in the vibrational partition functions (Table D.13).

We have used the bimolecular reaction rate constant obtained by Park *et al.* (2004), 2.3×10^{-12} cm^3 molecule^{-1} s^{-1} for the reaction between molecular oxygen and OH-isoprene, to represent the bimolecular reaction between our OH addition products and molecular oxygen. With the Park *et al.* (2004) reaction rate constant and a molecular oxygen concentration of 5.2×10^{18} molecule cm^{-3} the pseudo-first order reaction rate becomes 1.2×10^7 s^{-1}.

The "cold" reaction rate constants are estimated using transition state theory including the quantum tunneling given by

$$k_{TST} = \frac{k_B T}{h} \times \frac{Q_{TS}}{Q_R} \times e^{-\Delta E / k_B T} \tag{D.1}$$

where Q_R and Q_{TS} are the partition functions for the reactant, R, and the transition state, TS, respectively (Henriksen and Hansen, 2008). The rigid rotor and harmonic oscillator approximations have been used to calculate the partition functions. The energy ΔE is the energy difference between the transition state and the reactant. The constants, h and k_B, are the Planck constant and the Boltzmann constant, respectively. Tunneling was done with the Eckart approach (Eckart, 1930). The "cold" TST reaction rate constants are all much slower than the estimated pseudofirst order reaction rate constant of the OH-addition ISOPOOH products and molecular oxygen. With this reaction rate constant the bimolecular reaction dominates over the *cis*/*trans*-β-IEPOX production at atmospheric pressures.

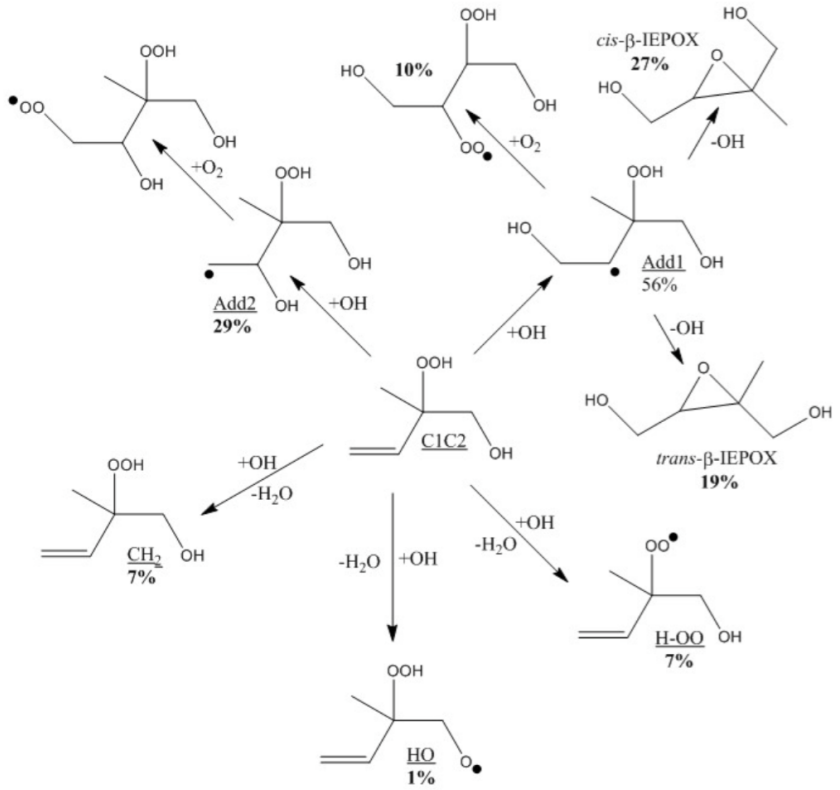

Figure D.17: The reactions of (1,2)-ISOPOOH with OH.

D.5.3.6 Mesmer Modeling

Our MESMER models have all the ISOPOOH+OH reactions along with the *cis*/trans-β-IEPOX production reactions that occur following the OH addition to the outer carbon. All the reactions are shown in Figure D.17 and Figure D.18 for the (1,2)-ISOPOOH and (4,3)-ISOPOOH molecules, respectively. We have used a grain size of 50 cm^{-1} and a grain span in the model of 30 kT (above the ISOPOOH+OH energy stationary point). We used a collisional activation/deactivation energy of 200 cm^{-1} per bath gas (N_2) collision, a temperature of 298.15 K, a pressure of 745 Torr and an OH concentration of 10^6 molecules cm^{-3}.

(1,2)-ISOPOOH+OH. The yields of each component are shown on Figure D.17. The total for the compounds' yields shown in bold add to 100%. Our model suggests that only a minor amount of the ISOPOOH-OH molecules are stabilized in the ISOPOOH-OH well. For the (1,2)-ISOPOOH+OH reaction in Figure D.17, we observe that the two addition reactions (Add1 and Add2) dominate over all the OH abstraction reactions. All OH abstraction reactions have yields that are lower than 7%. The OH addition to the inner carbon of the double bond has a yield of

29% of the total yield. After the inner OH addition, molecular oxygen adds and a hydroperoxydiol peroxy radical is produced.

The H-shift between the hydroperoxy hydrogen and the peroxy radical is calculated to be very fast ($\sim 10^4$ s^{-1}) - much faster than the bimolecular chemistry - so an equilibrium distribution between the two peroxy radicals will result. The calculations suggest that the peroxy radical on C2 will be favored.

The yield of the OH addition to the outer carbon is 56%. After the OH addition, the molecule can either produce *cis*/*trans*-β-IEPOX or a peroxy hydroperoxydiol molecule. Our model shows that the excess energy is high enough to overcome the energy barriers and to produce a high yield of β-IEPOX molecules. The 56% of OH addition to the outer carbon will divide into a production of a total yield of 19% *trans*-β-IEPOX, 27% *cis*-β-IEPOX molecule and 10% will add O_2 yielding a hydroperoxydiol peroxy radical. H-shift between the hydroperoxy hydrogen and the peroxy radical is also calculated to be very fast ($\sim 10^4$ s^{-1}) - much faster than the bimolecular chemistry and so, an equilibrium distribution between the two peroxy radicals will result.

(4,3)-ISOPOOH + OH. The calculated yields of each component are shown in Figure D.18. The total for the yields shown in bold add to 100%. OH addition to the outer carbon in the double bond dominates with a yield of 95% of the total yield. The yield of the OH abstraction reaction of the hydrogen α to the hydroperoxy group is around 3%, and all other reactions have production yields around 1% or lower. Of the 95% yield added to the outer carbon around 40% will produce the *cis*-β-IEPOX, 47% produce *trans*-β-IEPOX and around 8% will produce the hydroxyperoxydiol peroxy radical. The yield of *cis*/*trans*-β-IEPOX is much higher for (4,3)-ISOPOOH+OH compared to (1,2)-ISOPOOH+OH.

D.5.3.7 Further decomposition after the inner OH addition to the (1,2)-ISOPOOH molecule

Following addition of OH to the (1,2)-ISOPOOH *via* add2, we expect O_2 to add (C4OO) rather than formation of a 4 member epoxide-like compound. After O_2 addition, we find a rapid H-shift from the hydroperoxide group to the ROO (C2OO). A reaction scheme is shown in Figure D.19. We have looked at the (R,R)-enantiomer of the molecule and performed preliminary calculations with the M06-2X/aug-cc-pVTZ method. The calculated H-shift barrier height for this reaction is found to be 9.3 kcal mol^{-1}. The product is 0.4 kcal mol^{-1} lower than the reactant. The

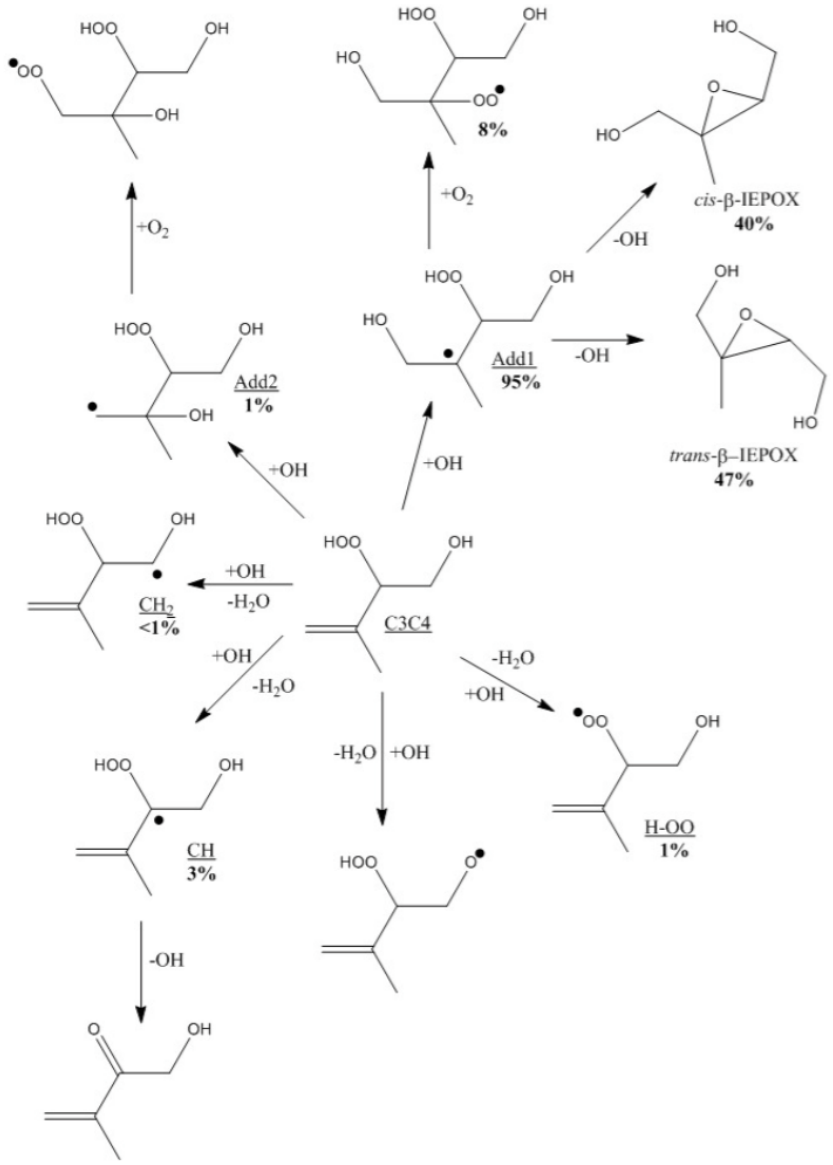

Figure D.18: The reactions of (4,3)-ISOPOOH with OH.

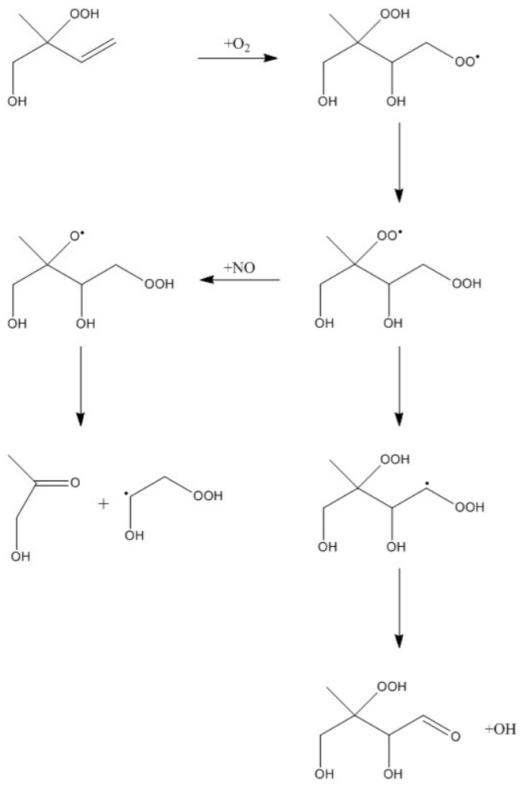

Figure D.19: The two possible H-shift reactions after the internal OH addition ($+O_2$) in the (1,2)-ISOPOOH molecule.

attachment of molecular oxygen releases an energy of 34.4 kcal mol^{-1} compared to the (1,2)-ISOPOOH-OH added product (inner addition), and the energy difference between the (1,2)-ISOPOOH+OH+O_2 and the molecule with the oxygen attached (reactant) is 63.8 kcal mol^{-1}. The "cold" TST reaction rate constants, including the Eckart tunneling correction, are 5.6×10^6 s^{-1} and 5.8×10^6 s^{-1} for the forward and backward H-shift reactions, respectively.

The second H-shift reaction would likely take the terminal hydrogen with the OOH group, and lead to loss of OH. It has a barrier height of 23.1 kcal mol^{-1} and a TST Eckart-corrected reaction rate constant of 1.2×10-4 s^{-1}. The energy of the final aldehyde + OH is almost 50.4 kcal mol^{-1} lower in energy than the transition state. The energetics are shown in Table D.14.

D.5.4 GEOS-Chem Calculations

The chemical mechanisms for the "Standard" and "Old" GEOS-Chem runs were identical except for the differences included in Table D.15. The complete "Standard" mechanism can be obtained at http://wiki.seas.harvard.edu/GEOS-Chem/index.php/

Species	δE+ZPVE (kcal mol^{-1})
(1,2)-ISOPOOH+OH+O_2	0.0
C4OO	-63.8
TS	-53.0
C2OO	-64.2
TS	-41.1
Aldehyde+OH	-91.5

Table D.14: The energetics (in kcal mol^{-1}) of the two H-shift reactions after the inner OH addition (+O_2) to the (1,2)-ISOPOOH molecule calculated with the M06-2X/aug-ccpVTZ method.

	"Standard"	"Old"
HO_2+RO_2 rate coefficient	$2.91\times10^{-13} \times e^{(1300/T)} \times [1\text{-}e^{(-0.245n}]$	$7.4\times10^{-13} \times e^{(700/T)}$
H-abstraction rate coefficient	$4.75\times10^{-12} \times e^{(200/T)}$	$3.8\times10^{-12} \times e^{(200/T)}$
H-abstraction yields	0.387ISOPOO + 0.613OH + 0.613HC_5	0.70ISOPOO + 0.300HC_5 + 0.300OH

Table D.15: Differences between the "Standard" and "Old" GEOS-Chem mechanisms.

New_isoprene_scheme.

The "Recommended" simulation run in GEOS-Chem included an increased ISOPOOH yield of 94% from the reaction of HO_2 with ISOPOO, as well as individually speciated ISOPOOH and IEPOX isomers. Listed below are the rates and products of individual reactions edited and added to the GEOS-Chem mechanism in the "Recommended" simulation to account for the isomers of ISOPOOH and IEPOX. In the GEOS-Chem mechanism, ISOPOOH is referred to as RIP; RIPA, RIPB, and RIPD refer to (1,2), (4,3), and delta (1,4 and 4,1) ISOPOOH respectively, while IEPOXA, IEPOXB, and IEPOXD refer to *trans-*β, *cis-*β, and δ IEPOX respectively. Temperature dependencies of rate constants were kept from the "Standard" GEOS-Chem mechanism.

RIO_2 + HO_2 $\rightarrow$ 0.628RIPA + 0.272RIPB + 0.037RIPD + 0.063(OH + CH_2O + HO_2) + 0.038MVK + 0.025MACR; k = $2.06 \times 10^{-13} \times e^{(1300/T)}$

RIPA + OH $\rightarrow$ 0.750RIO_2 + 0.250HC_5 + 0.125(OH + H_2O); k = $6.13 \times 10^{-12} \times e^{(200/T)}$

RIPA + OH $\rightarrow$ 0.850OH + 0.578IEPOXA + 0.272IEPOXB + 0.150HC_5OO; k = $1.70 \times 10^{-11} \times e^{(390/T)}$

RIPB + OH $\rightarrow$ 0.480RIO_2 + 0.520HC_5 + 0.26(OH + H_2O); k = $4.14 \times 10^{-12} \times e^{(200/T)}$

RIPB + OH $\rightarrow$ 1.000OH + 0.680IEPOXA + 0.320IEPOXB; k = $2.97 \times 10^{-11} \times e^{(390/T)}$

RIPD + OH $\rightarrow$ 0.250RIO_2 + 0.750HC_5 + 0.375(OH + H_2O); k = $5.11 \times 10^{-12} \times e^{(200/T)}$

RIPD + OH $\rightarrow$ 0.500OH + 0.500IEPOXD + 0.500HC_5OO; k = $2.92 \times 10^{-11} \times e^{(390/T)}$

IEPOXA + OH $\rightarrow$ IEPOXOO; k = $3.73 \times 10^{-11} \times e^{(-400/T)}$

IEPOXB + OH $\rightarrow$ IEPOXOO; k = $5.79 \times 10^{-11} \times e^{(-400/T)}$

IEPOXD + OH $\rightarrow$ IEPOXOO; k = $3.20 \times 10^{-11} \times e^{(-400/T)}$

Other reactions involving RIP and IEPOX in the original GEOS-Chem mechanism, including deposition and photolysis, were simply updated to apply to each individual isomer of the two compounds.